Formation Mechanism of Hydrogenated Silicon Clusters during Thermal Decomposition of Disilane

Kenichi Tonokura,* Tetsuya Murasaki, and Mitsuo Koshi†

Department of Chemical System Engineering, School of Engineering, The University of Tokyo, 7-3-1 Hongo, Bunkyo-ku, Tokyo 113-8656, Japan

Received: August 19, 2001; In Final Form: November 19, 2001

Hydrogenated silicon clusters (Si_nH_m) were detected during the thermal decomposition of disilane in a flow reactor by using time-of-flight (TOF) mass spectrometry coupled with vacuum ultraviolet (VUV) photoionization at a temperature range of 680−860 K and total pressures of 20−40 Torr. Si_nH_m clusters were photoionized by the VUV radiation at 10.2 eV (121.6 nm). The Si_nH_{2n+2} ($n \geq 2$), Si_nH_{2n} ($n \geq 2$), Si_nH_{2n-2} ($n \geq 5$), and Si_nH_{2n-4} ($n \geq 5$) containing up to 10 silicon atoms were observed as gas-phase products during the disilane pyrolysis, while no ion signal due to Si_1 species such as Si, SiH, SiH_2, and SiH_3 was detected. Energetics for the disilane unimolecular decomposition has been calculated at the Gaussian-3 (G3)//B3LYP level of theory. On the basis of a kinetic model proposed by Swihart and Girshick [*J. Phys. Chem. B* **1999**, *103*, 64], the gas-phase kinetic simulation has been performed to analyze the formation mechanism of hydrogenated silicon clusters in the thermal decomposition of disilane. Temperature and time dependences of disilane loss and hydrogenated silicon cluster formation were compared with the results of kinetic simulation. The formation processes of $Si_{2n}H_{2n}$ and Si_nH_{2n-2}, which have linear or cyclic and polycyclic structures, were suggested to be the key steps for the large cluster growth.

Introduction

The formation mechanism of hydrogenated silicon clusters generated during the thermal decomposition of silanes is of fundamental interest as well as technological importance in the semiconductor industry. Disilane is considered as an interesting source for the thermal chemical vapor deposition (CVD) of epitaxial silicon because it pyrolyzes at lower temperatures than silane. The primary decomposition processes during disilane pyrolysis result from the molecular elimination of silane or hydrogen to form silylenes (Figure 1 and Table 1).[1−11]

$$Si_2H_6 \rightarrow SiH_4 + SiH_2 \quad (1)$$

$$\rightarrow H_2 + H_3SiSiH \quad (2)$$

The heats of reaction for these two processes are nearly the same. Subsequently, silylenes (Si_nH_{2n}) may insert into a Si−H bond of silanes (Si_nH_{2n+2}); thereby, higher silanes are generated.

$$Si_nH_{2n} + Si_mH_{2m+2} \rightarrow Si_{n+m}H_{2(n+m+1)} \quad (3)$$

In the case of silylsilylene (H_3SiSiH) an insertion reaction into the Si−H bond competes with an isomerization to disilene ($H_2Si{=}SiH_2$).

$$H_3SiSiH \rightarrow H_2Si{=}SiH_2 \quad (4)$$

The products formed in reactions 3 and 4 may undergo further decomposition and reactions that lead to the formation of hydrogenated silicon clusters.

Chemical kinetic modeling of hydrogenated silicon pyrolysis, including reactions that lead to the formation of hydrogenated silicon clusters, has been widely studied.[12−15] The reaction mechanisms involve a large number of reaction steps including unimolecular decomposition, abstraction, elimination, insertion, and isomerization reactions. Yuuki et al.[12] constructed a simple gaseous reaction model involving 11 elementary reactions for 10 chemical species (up to five silicon atoms) for silane and disilane pyrolysis. Giunta et al.[13] proposed a larger mechanism that included linear silane, silylene, and silenes with up to 10 silicon atoms and isomerizations of larger silylenes (H_3SiSiH and larger) to form disilenes. Frenklach et al.[14] developed a detailed chemical kinetic model including 117 elementary reactions of 42 chemical species for the formation of silicon particles by hydrogenated silicon clustering at higher temperatures. In both of these latter studies, the rate coefficients for the reactions involving silanes and silylenes containing more than two silicon atoms were assumed to be identical to those for the analogous reaction of disilane. Recently, Swihart and Girshick[15] pointed out that the hydrogenated silicons with rings and more complex three-dimensional structures would play an important role in the growth mechanism of a hydrogenated silicon cluster. They presented a reaction mechanism consisting of reversible reactions among hydrogenated silicons containing up to 10 silicon atoms and irreversible formation of hydrogenated silicons containing 11−20 silicon atoms in the absence of any surface reactions. The formation of an eight-silicon-containing cluster was predicted to be a key reaction path and a kinetic bottleneck.

Species such as silylene and disilene have been considered as key intermediates in the thermal CVD of silicon. Disilyne (Si_2H_2) was also suggested as a key intermediate leading to Si-thin-film growth in CVD because this species is expected to be the decomposition product of disilane.[2,8,11] Thus, identification

* To whom correspondence should be addressed. E-mail: tonokura@reac.t.u-tokyo.ac.jp.
† E-mail: koshi@chemsys.t.u-tokyo.ac.jp.

10.1021/jp015523n CCC: $22.00
Published on Web 12/20/2001

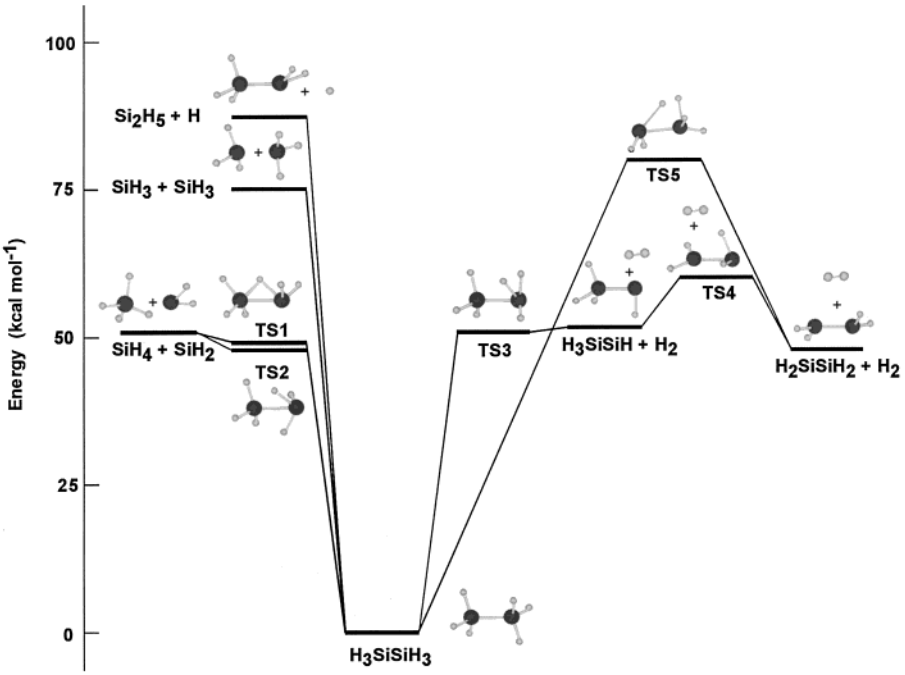

Figure 1. Energy diagram for the unimolecular decomposition of disilane calculated at the G3//B3LYP level of theory.

TABLE 1: Energetics for Thermal Decomposition of Si_2H_6

	ΔH_r (kcal mol^{-1})	
	G3//B3LYP	exp
H_3SiSiH_3		
$\rightarrow SiH_4 + SiH_2$	52.1	54.3
$\rightarrow H_3SiSiH + H_2$	54.0	55.5
$\rightarrow H_2SiSiH_2 + H_2$	46.7	46.6
$\rightarrow SiH_3 + SiH_3$	75.3	76.7
$\rightarrow Si_2H_5 + H$	88.2	89.3
$\rightarrow SiH_4 + SiH_2$ (TS1)	43.7	53.4
$\rightarrow SiH_4 + SiH_2$ (TS2)	43.1	
$\rightarrow H_3SiSiH + H_2$ (TS3)	51.1	56.4
$\rightarrow H_2SiSiH_2 + H_2$ (TS5)	80.5	
$H_3SiSiH + H_2$		
$\rightarrow H_2SiSiH_2 + H_2$ (TS4)	7.0	5.3
H_3SiSiH_3 (staggered)		
$\rightarrow H_3SiSiH_3$ (eclipsed)	0.95	1.26

and understanding of the chemical kinetics of reactive species generated during the disilane pyrolysis are considered to be essential for an elucidation of the clustering mechanism of hydrogenated silicon. Detection of gas-phase intermediates at lower temperatures (below 1000 K) has been performed by using laser-induced fluorescence (LIF),[16] mass spectrometry,[17−19] and resonance-enhanced multiphoton ionization (REMPI).[20] Ho et al.[16] measured Si atoms during the silane and disilane pyrolysis in a rotating disk CVD reactor using LIF. They constructed a kinetic model of CVD from silane and disilane containing up to Si_3 spices. The reactions of $H_3SiSiH \leftrightarrow Si + SiH_4$ and $H_3SiSiH + SiH_2 \leftrightarrow Si + Si_2H_6$ were proposed as a source of gas-phase Si atoms in the system. Simon et al.[19] confirmed the formation of Si_nH_{2n+2} ($n = 3-5$) in the thermal decomposition of disilane using the quadrupole mass spectrometric technique. Because the mass spectrum measured using electron impact ionization at 70 eV contains the ionic fragments, there was difficulty in the confirmation of other hydrogenated silicon products. Johannes and Ekerdt[20] used a multiphoton ionization (MPI) technique to detect silicon intermediates in the gas-phase thermal reactions during disilane pyrolysis. The fragments of higher molecular weight silanes and disilenes have been detected by MPI with masses 2 (H_2^+), 30 (SiH_2^+), and 60 ($Si_2H_4^+$) being associated with higher molecular weight fragments. Weerts et al.[17] used a quadrupole mass spectrometer at an ionization energy of 70 eV for on-line-gas-phase analysis. Onischuk et al.[18] measured the time dependences of silane consumption and disilane and trisilane formation in silane thermal decomposition by using a quadrupole mass spectrometer. They qualitatively explained silane conversion and disilane formation on the basis of a simple kinetic scheme. The daughter ions may result from the fragmentation of higher mass molecules in the ionization processes, which are obstacles to analysis in the thermal decomposition of disilane using the conventional mass spectrometric techniques. Therefore, the intermediates formed by the disilane thermal decomposition have not been well-understood experimentally. More recently, time-of-flight (TOF) mass spectrometry coupled with vacuum ultraviolet (VUV) laser photoionization was employed for the determination of gas-phase molecules formed after the thermal decomposition of disilane.[21] In this method, the gas-phase intermediates were detected without fragmentation in the ionization processes.

In this paper, we examine the mechanism of the thermal decomposition of disilane, including reactions that lead to the formation of hydrogenated silicon clusters. The temperature and time dependences of the formation of the hydrogenated silicon clusters containing up to 10 Si atoms were measured by using TOF mass spectrometry coupled with VUV laser photoionization. The experimental data are qualitatively interpreted with the use of a gas-phase chemical kinetic model, which includes hydrogenated silicon clusters with linear, cyclic, and polycyclic structures proposed by Swihart and Girshick.[15]

Experimental Section

Experiments were performed using a molecular beam sampling technique combined with TOF mass spectrometry. The method has been described in detail previously.[21] Briefly, the apparatus consists of a quartz reaction tube incorporated into a source chamber of the molecular beam machine, which is equipped with the Wiley−McLaren-[22] and reflectron-type[23] TOF mass spectrometer. The reactant gas mixtures were slowly flowed in the quartz reactor (i.d. = 15 mm) with a sampling

hole of 200 μm diameter placed at the center of the reactor. The products of thermal decomposition were continuously sampled through the pinhole and were collimated by a 1.0 mm orifice skimmer mounted 4.0 mm from the pinhole in the reaction tube. The molecular beam was introduced into the TOF mass spectrometer. The source chamber was pumped by a 1500 L/s diffusion pump to a chamber base pressure of 10^{-7} Torr. The detection chamber was pumped by a turbo molecular pump with a pumping speed of 500 L/s to a chamber base pressure of 10^{-8} Torr. During the experiment, the typical pressures in the beam source and in the detection chamber were kept at $\sim 5 \times 10^{-5}$ and $\sim 2 \times 10^{-6}$ Torr, respectively. An Einzel lens and deflectors were located just above ion acceleration regions. For elevated-temperature experiments, Nichrome ribbon was coiled around the reaction tube. The temperature profiles inside the reactor were measured using a movable type K thermocouple. The maximum deviation from the base temperature in a usable length of 8 cm upstream from the pinhole was $\pm 3\%$.

The ionization was accomplished by the photoionization at 10.2 eV (121.6 nm). Coherent VUV laser radiation was obtained by frequency tripling in a phase-matched Kr/Ar gas mixture adjusted to achieve optimum phase matching.[24] A frequency-tripling gas cell was sealed at the end opposite of a MgF_2 lens (70 mm focal length at 121.6 nm) by a fused silica window. A lens with a focal length of 15 cm was used to focus the output ($1-8$ mJ pulse^{-1}) of the excimer-pumped dye laser (Lambda Physik LPX 110 + Lambda Physik LPD 3002) at 364.6 nm in the cell containing the rare gas mixture. The VUV and the residual dye laser light passed through the MgF_2 lens and onto the molecular beam. The spot size of the VUV laser light at the point of the molecular beam was about 1 mm. The focusing MgF_2 lens had a lower refractive index ($\eta = 1.6275$ at 121.6 nm compared with $\eta = 1.386$ at 364.6 nm) at the longer wavelength; hence, the residual UV beam was mildly divergent. The VUV laser light was directed into a NO-contained photoionization cell. The NO molecule has an ionization potential of 9.24 eV, and thus, the incident VUV photon at 10.2 eV can ionize the NO molecules. The resultant photocurrent by ejected electron or ionized NO was monitored to measure the relative intensity of the VUV light ($\sim 10^8-10^{10}$ photons pulse^{-1}). The ion signal was detected by a two-stage microchannel plate (MCP; Hamamatsu F4655-10). The output of the signal from the MCP was fed to a 500 MHz, 1 GS/s digital oscilloscope (Tektronix TDS 520C) and transferred to a Pentium personal computer via a general purpose interface bus. The TOF spectra were accumulated over 2000 laser pulses.

The dependence of the $Si_2H_6^+$ signal versus VUV laser power gives a slope of 0.91 ± 0.02, indicating that the ionization resulting from the multiphoton process by the combination of VUV and UV laser light seems negligible. The experiments were carried out at lower VUV laser power to prevent the multiphoton ionization processes by VUV radiation. From the results of Ruscic et al.[25] and Kameta et al.,[26] the photoionization cross section of disilane at 10.2 eV is estimated to be ca. 3×10^{-17} cm^2 molecule^{-1}. When the 2 mJ of the UV light is introduced into the VUV generation cell, the intensity of VUV light is estimated to be 10^8 photons per pulse. Under this condition, a detection limit for disilane concentration in the reaction tube is estimated to be ca. 10^{12} molecules cm^{-3}. Table 2 shows ionization potentials of Si compounds up to five silicon atoms and appearance potentials of species produced by the photoionization of Si_2H_6.[25,27−32]

Diluted mixtures of disilane (Nippon Sanso, 1.05% Si_2H_6/98.95% He and 0.97% Si_2H_6/99.03% Ar), He (Nippon Sanso, 99.9999%), and Ar (Nippon Sanso, 99.9999%) were used without further purification. The gases were regulated by calibrated mass flow controllers (KOFLOC 3650). The gas pressures in the reaction tube were measured with a capacitance manometer (MKS Baratron 622A). Total pressure in the reaction tube was maintained at 20−40 Torr. Reagent concentrations were calculated from the total pressure and the calibrated flow rates. The residence times (0.01−0.5 s) were controlled by linear flow rates.

TABLE 2: Ionization Potentials of Si Compounds and Appearance Potentials of Species Produced by Photoionization of Si_2H_6

compound	ionization potential (eV)	appearance potential (eV)
Si	8.15[a]	15[d]
SiH	7.91[b]	14.0[c]
SiH_2	9.15[b]	11.95[g]
SiH_3	8.01[b]	<11.72[d]
SiH_4	11.00[b]	
Si_2	7.9−8.1[a]	<14.5[d]
Si_2H	8.10[d]	15.0[d]
$Si(H_2)Si$	8.20[c]	<11.57[e]
$SiSiH_3$	<7.59[c]	<12.70[e]
H_2SiSiH_2	8.09[c]	<10.04[e]
H_3SiSiH	8.40[d]	<10.81[e]
H_3SiSiH_2	7.60[c]	<11.41[e]
Si_2H_6	9.74[e]	
Si_3	<8.49[a]	
Si_3H_8	9.97[f]	
Si_4	7.97−8.49[a]	
n-Si_4H_{10}	9.62[f]	
Si_5	7.97−8.49[a]	
n-Si_5H_{12}	9.36[f]	

[a] Reference 27. [b] Reference 28. [c] Reference 29. [d] Reference 30. [e] Reference 25. [f] Reference 31.Vertical ionization potential. [g] Reference 32.

Computational Methods

Quantum chemical calculations were carried out using the Gaussian 98 series of programs.[33] All calculations used density functional theory (DFT) with the B3LYP functional. This DFT uses Beck's gradient-corrected exchange functional,[34] Lee−Yang−Parr's gradient-corrected correlation functional,[35] and Beck's three parameter hybrid HF/DFT method[36] using Lee−Yang−Parr's correlational functional. The geometry optimization and frequency calculations used the 6-31G(d) basis set. Gaussian-3 (G3)//B3LYP calculations[37] were performed to obtain the energies for molecules, ions, and transition states. In the G3//B3LYP method the initial geometries and zero-point energies are obtained from B3LYP density functional theory [B3LYP/6-31G(d)].

Kinetic modeling was carried out with CHEMKIN-III program packages[38] using a set of reactions to simulate the gas-phase chemical kinetics of the thermal decomposition of Si_2H_6 at each experimental temperature. The chemical kinetic model has a total of 2614 gas-phase reactions involving 221 chemical species up to 20 silicon atoms, which is proposed by Swihart and Girshick;[15] the time profiles of the hydrogenated silicon cluster formation were calculated numerically, as discussed later.

Results

Unimolecular Decomposition of Disilane. An initial step of the hydrogenated silicon cluster formation during the disilane pyrolysis is the unimolecular decomposition of disilane. Figure 1 and Table 1 show the energetics of the unimolecular decomposition of disilane calculated at the G3//B3LYP level

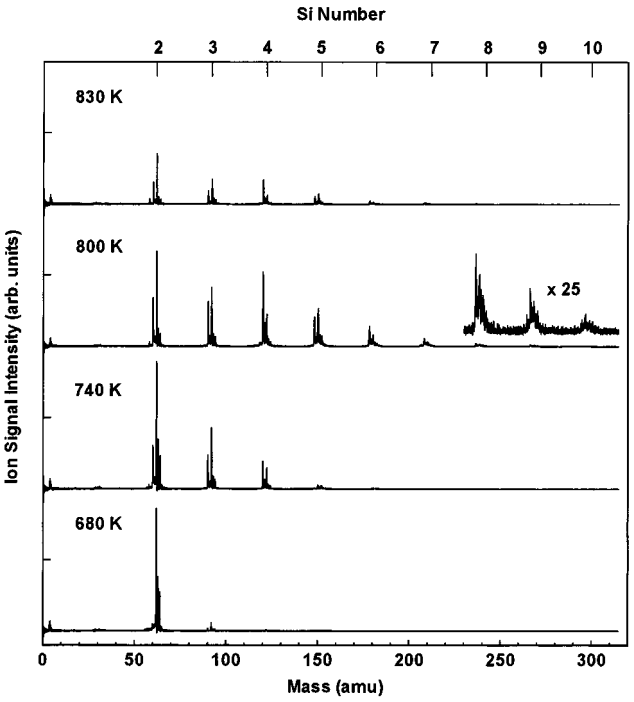

Figure 2. Photoionization mass spectra of the thermal decomposition products of disilane at reaction temperatures of 680, 740, 800, and 830 K. The spectra were obtained with a residence time of 0.4 s. The initial concentration of disilane in the flow reactor is 1.3×10^{16} molecules cm^{-3} at 40 Torr total pressure.

of theory. The results are consistent with the previous studies cited above. Silylene and silylsilylene formation channels are found to be competitive; predicted reaction enthalpies are calculated to be within a 2 kcal mol^{-1} range.

There are two silylene elimination geometries in the disilane dissociation reaction 1 (TS1 and TS2). The barriers for both silylene elimination channels are actually slightly below the separated products, $SiH_2 + SiH_4$. The existence of such a van der Waals complex has already been pointed out by Becerra et al.[39] Both reaction channels have long-range minima between the transition state and products, $SiH_2 + SiH_4$. The three-centered 1,1 H_2 elimination to produce silylsilylene occurs via a transition state (TS3) with activation energy near the heat of reaction. Direct disilene formation via a four-centered 1,2 H_2 elimination process (TS5) requires a large activation energy of 80.5 kcal mol^{-1}. If disilene is produced in the disilane pyrolysis, the most likely route is via isomerization from silylsilylene. The heat of formation of disilene is 7.3 kcal mol^{-1} lower than that of silylsilylene at the G3//B3LYP calculations. Becerra and Walsh[7] estimated the Arrhenius parameter for this isomerization reaction. They obtained an experimentally based estimate of $E_a = 5.3 \pm 2.0$ kcal mol^{-1}. The energy barrier (TS4) for the isomerization of silylsilylene to disilene estimated by G3// B3LYP calculations is 7.0 kcal mol^{-1}, consistent with the estimate of Becerra and Walsh.[7]

Mass Spectrometric Detection of Hydrogenated Silicon Clusters. Figure 2 shows the photoionization mass spectra obtained with the ionization energy of 10.2 eV during the disilane pyrolysis over a temperature range of 680−830 K at a total pressure of 40 Torr. Except for SiH_4, most of the Si_nH_m species are able to photoionize at 10.2 eV photon energy, as shown in Table 2. The ionization potential of linear silanes shifts to lower energy with increasing Si number. The ion signals up to Si_{10} species were observed at a reaction temperature of 800 K. The mass spectra have no fragmentation in the photoionization processes of disilane at 10.2 eV as has been reported in the literature.[21] In our previous threshold ionization experiment of Si_3H_8 by the electron impact at 11 eV, relatively weak fragmentation signals at $m/z = 60$ and 62 have been observed.[40] It is expected that the photoionization of Si_2H_6 and Si_3H_8 at 10.2 eV would not produce the fragment ion.

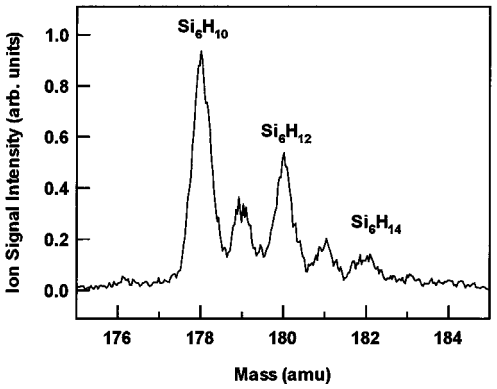

Figure 3. Photoionization mass spectrum of Si_6H_m species during the thermal decomposition of disilane at 800 K with residence time $t =$ 0.4 s.

Disilane pyrolysis produces higher silanes (Si_nH_{2n+2}), silenes ($H_2Si{=}SiHSi_{n-2}H_{2n-3}$), and silylenes ($HSi{-}Si_{n-1}H_{2n-1}$).[41] A typical example of an observation of Si_nH_{2n} and Si_nH_{2n-2} for Si_6 species is shown in Figure 3. The formation of Si_6H_{10} and Si_6H_{12} was clearly identified. There are small peaks between the Si_6H_{10}, Si_6H_{12}, and Si_6H_{14} (at 179 and 181 amu) due to the natural abundance of ^{29}Si and ^{30}Si. Half of the signal of Si_6H_{12} at 180 amu is due to the isotopes of Si. Figure 4 presents the ion signal intensity of several Si_nH_m species as a function of temperature obtained with a constant residence time of 0.4 s. The ion signal of Si_2H_6 decreases with increasing temperature as a result of more promotion of unimolecular decomposition at higher temperature. Except for Si_2H_6, the signals reached a maximum between approximately 750 and 800 K. The threshold temperature and peak position shifted to the higher temperature region with increasing size of hydrogenated silicon clusters. The ion signal profiles became narrower with the increasing number of Si atoms in the cluster. The ion signals were found to go down above 860 K because silicon nanoparticles deposited on the reactor wall and filled the pinhole.

We also observed time profiles for the reduction of Si_2H_6 and the production of Si_nH_{2-2n} ($n \geq 5$), Si_nH_{2n} ($n \geq 2$), and Si_nH_{2n+2} ($n \geq 3$) in the time range of 0.01−0.4 s at several temperatures. Figure 5 shows the dependence of Si_2H_6 depletion and Si_nH_m ($n = 2{-}7$) formation on the residence time at 770 K. The $Si_2H_6^+$ intensity was decreased by the promotion of unimolecular decomposition as a function of residence time, while the rise of signal intensity of Si_nH_m species assigned to the formation of Si_nH_m species was observed.

Kinetic Simulations. The gas-phase reaction mechanism of the CVD of silicon proposed by Swihart and Girshick,[15] which is based on the reactions and rate parameters presented by Ho et al.[16] for reactions among species containing one or two silicon atoms, was used to simulate the formation mechanism of hydrogenated silicon clusters. They determined the enthalpies and entropies of hydrogenated silicon from a group additivity method. The reaction mechanism included all of the possible reactions of these five types for which all of the participating species were among those summarized in Table 3. The gas-phase reactions were incorporated into the model using the SENKIN program[42] from the CHEMKIN family of codes. Figures 6 and 7 show the results of the simulation using the

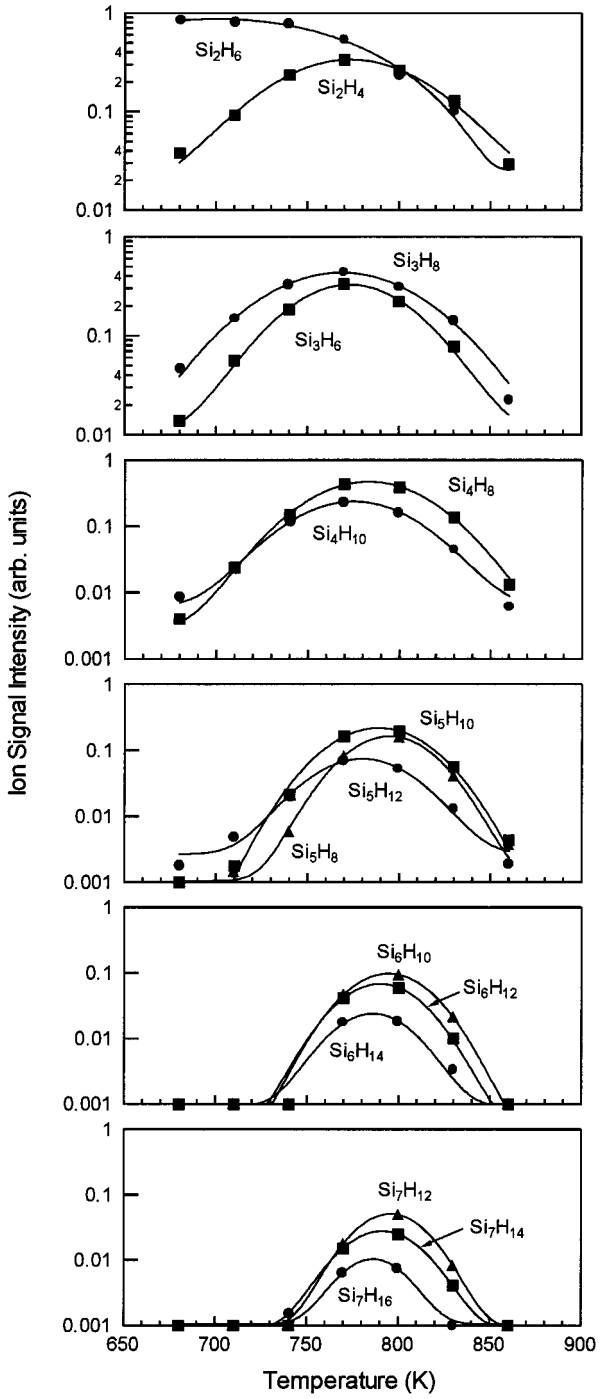

Figure 4. Ion signal intensity of Si_nH_m species ($n = 2-7$) as a function of temperature: (●) Si_nH_{2n+2}; (■) Si_nH_{2n}; (▲) Si_nH_{2n-2}. The curves are a spline function fitted to the data. Residence time $t = 0.4$ s.

model proposed by Swihart and Girshick. The comparisons of experimental data of Si_2H_6 with modeling results are given in Figure 8.

Discussion

Formation of Hydrogenated Silicon Clusters. *Si_1 Species.* The ion signals of Si_1 species such as Si (mass-28), silylidyne (SiH, mass-29), silylene (SiH_2, mass-30), or silyl (SiH_3, mass-31) were not detected during the disilane pyrolysis. Si, SiH, and SiH_3 are not predicted to form as a primary product in the thermal decomposition of disilane. The photoionization cross section of Si, 4×10^{-17} cm^2 molecule^{-1},[43] is the almost same as that of disilane. Ho et al.[16] observed Si atoms during the

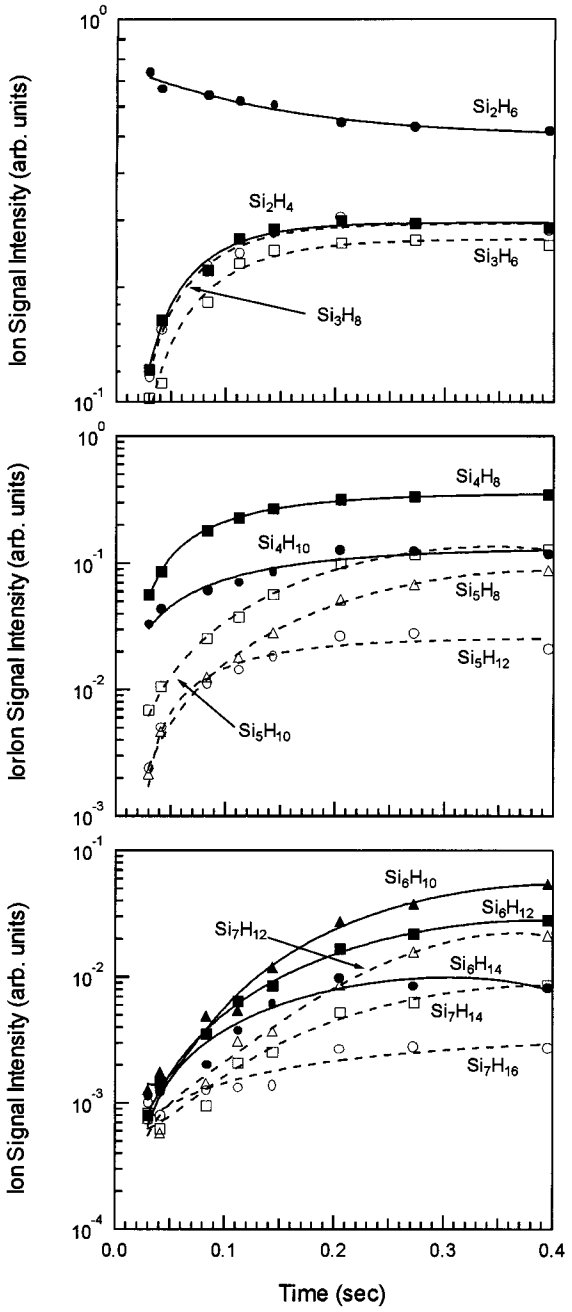

Figure 5. Concentration profiles of Si_nH_m species as a function of residence time: (● and ○) Si_nH_{2n+2}; (■ and □) Si_nH_{2n} ; (▲ and △) Si_nH_{2n-2}. The curves are a spline function fitted to data. Reaction temperature $T = 770$ K.

CVD of disilane by LIF. They concluded that the $H_3SiSiH \leftrightarrow Si + SiH_4$ and $H_3SiSiH + SiH_2 \leftrightarrow Si + Si_2H_6$ reactions lead to Si atom formation. Under their predictions, the concentration of Si atom is $<10^7$ atoms cm^{-3}, which is lower than the detectable concentration ($10^{10}-10^{11}$ cm^{-3}) of disilane in the present study. SiH_2 is known to be very reactive and the rate constant for the reaction of SiH_2 with Si_2H_6 was reported to be 4.5×10^{-10} cm^3 molecule^{-1} s^{-1} at 590 K.[44] Under the present experimental conditions, a kinetic lifetime of SiH_2 is estimated to be $<1.6 \times 10^{-7}$ s^{-1}; therefore, a steady-state concentration of SiH_2 is predicted to be low, which is proved by a kinetic simulation (Figure 6). The electron impact ionization cross sections of SiH, SiH_2, and SiH_3[45] at 10 eV were reported to be 5×10^{-17}, 2×10^{-17}, and 2×10^{-17} cm^2 molecule^{-1}, respectively, while there are no data for the photoionization cross

TABLE 3: Hydrogenated Silicons in Mechanism[a]

species	Si_1	Si_2	Si_3	Si_4	Si_5	...	Si_n	structure
silane	SiH_4	Si_2H_6	Si_3H_8	Si_4H_{10}	Si_5H_{12}	...	Si_nH_{2n+2}	chain
			Si_3H_6	Si_4H_8	Si_5H_{10}	...	Si_nH_{2n}	ring
					Si_5H_8	...	Si_nH_{2n-2}	2 rings
						...	Si_nH_{2n-4}	3 rings
silene A		Si_2H_4A	Si_3H_6A	Si_4H_8A	$Si_5H_{10}A$	...	$Si_nH_{2n}A$	chain
			Si_3H_4A	Si_4H_6A	Si_5H_8A	...	$Si_nH_{2n-2}A$	ring
					Si_5H_6A	...	$Si_nH_{2n-4}A$	2 rings
						...	$Si_nH_{2n-6}A$	3 rings
silylene B	SiH_2B	Si_2H_4B	Si_3H_6B	Si_4H_8B	$Si_5H_{10}B$	...	$Si_nH_{2n}B$	chain
			Si_3H_4B	Si_4H_6B	Si_5H_8B	...	$Si_nH_{2n-2}B$	ring
					Si_5H_6B	...	$Si_nH_{2n-4}B$	2 rings
						...	$Si_nH_{2n-6}B$	3 rings

[a] Molecules without a suffix are fully saturated silanes. Molecules with an A suffix are silenes. Molecules with a B suffix are silylenes. No special notation is used to differentiate between acyclic, cyclic, and polycyclic molecules.

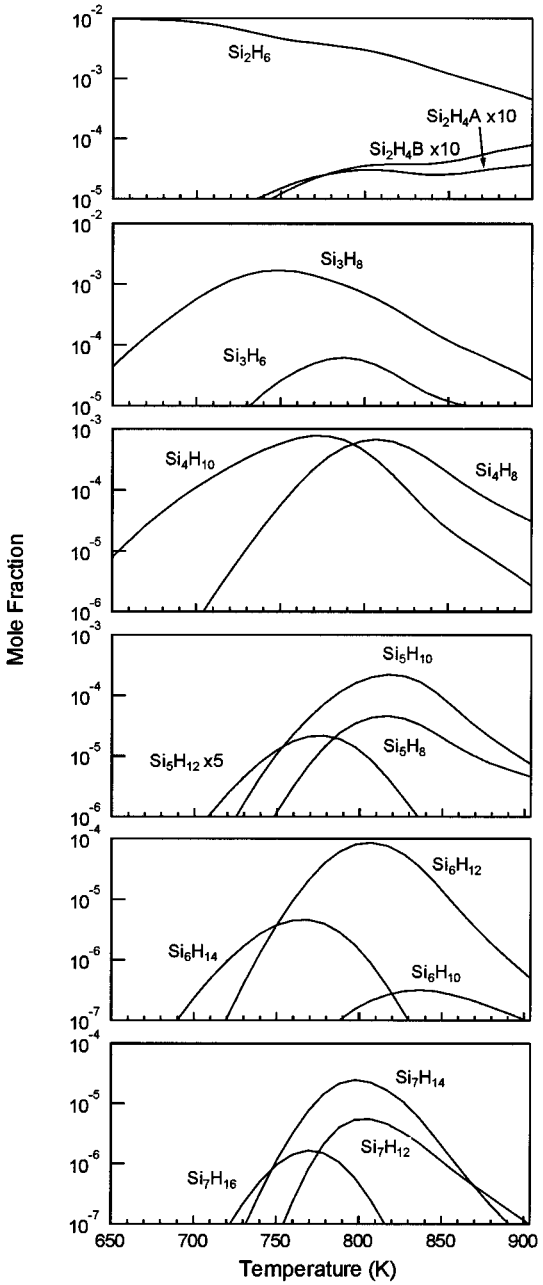

Figure 6. Mole fractions of Si_nH_m species as a function of temperature predicted by a Swihart and Girshick model for 1% of disilane in He at 40 Torr and time $t = 0.4$ s.

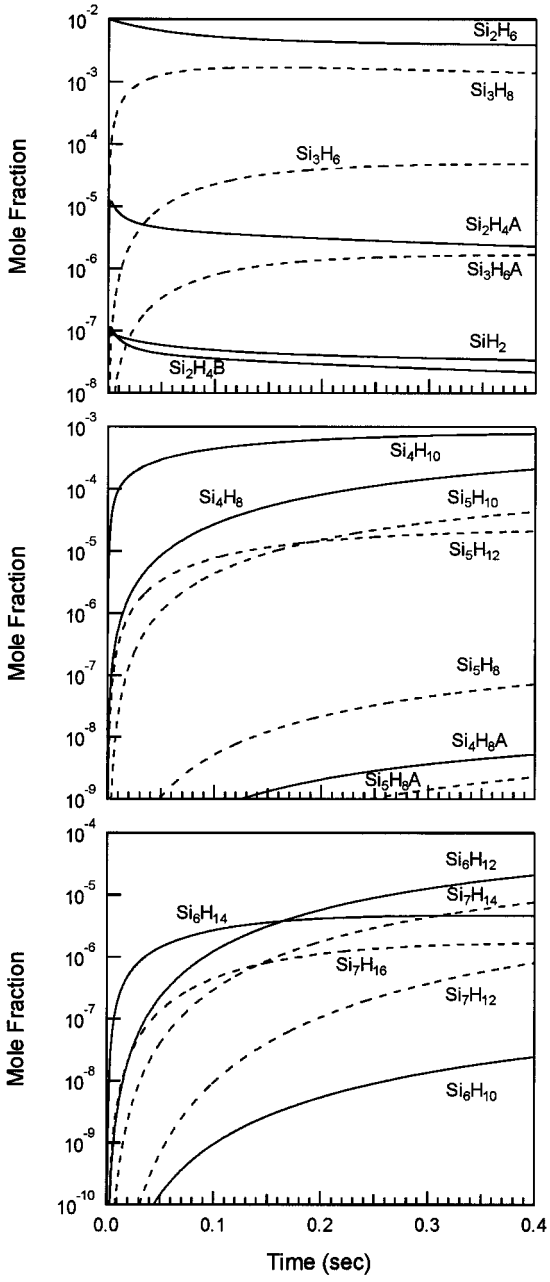

Figure 7. Mole fractions of Si_nH_m species as a function of reaction time predicted by a Swihart and Girshick model for 1% of disilane in He at 40 Torr and temperature $T = 770$ K.

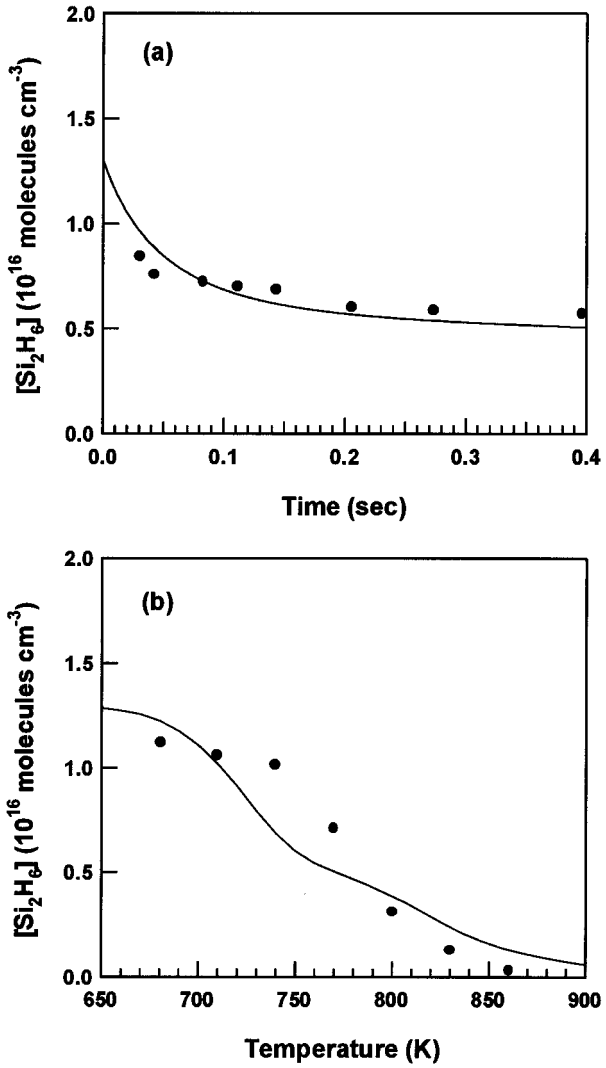

Figure 8. Comparison of experimental concentration of disilane (closed circles) and modeling results (solid curve): (a) disilane concentration versus reaction time t at 770 K; (b) disilane concentration versus reaction temperature at reaction time $t = 0.4$ s.

sections of these species. The electron impact ionization cross section of Si_2H_6 of 5.4×10^{-18} cm^2 molecule^{-1} at 11 eV[46] is $^1/_{20}$ of the photoionization cross section, 1.1×10^{-16} cm^2 molecule^{-1}. Therefore, the cross sections of Si species by photonionization around 10 eV may be the same or larger than those by electron impact. From the signal-to-noise ratio and the expected ionization cross sections, the upper limit of the concentration of Si_1 species is estimated to be $\leq 10^{12}$ molecules cm^{-3}.

Si_2 Species. Si_2H_4 was detected as a primary product in the thermal decomposition of disilane, and a small amount of Si_2H_2 was observed. Si_2H_4 is mainly produced from the thermal decomposition of disilane and higher silanes produced from reaction 3. As a possibility of $Si_2H_4^+$ observation, the fragmentation from higher Si_n species in the ionization process is considered. No fragmentation occurs in the photoionization of Si_2H_6 and Si_3H_8 at 10.2 eV, as discussed above. Because the time dependence of Si_2H_4 is close to that of Si_3H_6, $Si_2H_4^+$ could be caused by the fragmentation of Si_3H_6 species. The appearance potential of the $Si_2H_4^+ + H_2$ channel in the photoionization processes of Si_3H_6 is 10.99 eV.[47] Although this process would be ruled out, the fragmentation from the higher hydrogenated silicons cannot be negligible.

There are two paths for the production of Si_2H_2. One is a reaction of Si(^{3}P) + SiH_4 to produce Si_2H_2 and H_2 with $\Delta H = -23.0$ kcal mol^{-1}.[47] Another is a unimolecular decomposition of disilene with $\Delta H = 25.7$ kcal mol^{-1}.[47] Although Si_2H_2 may be produced during the thermal decomposition processes, there is experimental evidence that most of the Si_2H_2 is produced by thermal desorption from the hydrogenated amorphous Si film produced in the decomposition of disilane.[21]

Si_n($n \geq 3$) Species. The global minimum on the Si_3H_6 ground-state surface has been predicted to be cyclotrisilane by ab initio molecular orbital calculations.[48] Swihart and Girshick[15] suggested that cyclic hydrogenated silicons (Si_nH_{2n}, Si_nH_{2n-2}, Si_nH_{2n-4}, etc.) become important in the formation of the higher hydrogenated silicon clusters. For Si_6H_{10}, two monocyclo isomers and one bicyclo isomer were predicted, and the latter isomer is the most stable. The most stable isomer of Si_6H_{12} was predicted to be cyclohexasilane. The ion signal intensity of Si_6H_{12} and Si_6H_{10} is stronger than that of Si_6H_{14} (hexasilane) at 800 K, which suggests the formation of cyclic hydrogenated silicons. The increased intensity ratios of $[Si_nH_{2n}]/[Si_nH_{2n+2}]$ and $[Si_nH_{2n-2}]/[Si_nH_{2n+2}]$ with increasing number of Si atoms suggest that multi-H_2-elimination processes play an important role in the formation of higher hydrogenated silicon clusters.

Because a sticking coefficient for Si_2H_6 species under the present experimental conditions is quite small,[18] the contribution of heterogeneous decomposition of disilane is expected to be negligible. To examine the contribution of the heterogeneous reactions in the production of Si_nH_m, two buffer gases of He and Ar were used to control the diffusion rate. No significant difference in the mass spectra has been observed between the two buffer gases.

Kinetic Simulations. As can be seen in Figure 8, the time and temperature dependences of the experimental disilane concentration correlate reasonably with the modeling results. In comparison between the experimental data and the modeling results, the differences between the concentration profiles of Si_2H_4 species are clear. For temperature dependence (Figures 4 and 6), the experimental Si_2H_4 concentration decreases after reaching a concentration maximum around 770 K, while the modeling results show increasing disilane concentration at temperatures higher than 800 K. For the time dependencies of Si_2H_4 concentrations, although the experimental concentration rises gradually (Figure 5), the modeling results exhibit the steep rise at the initial stage and gradual decay (Figure 7). The time-dependent profile of Si_2H_4 is sensitive to the rate parameters of reaction 2. There have been two experimental determinations of the rate parameters for the reaction 2 to produce H_3SiSiH and H_2.[1,2] Bowrey and Purnell estimated the $(k_2/k_1)_{600K,\infty} = 3.0 \times 10^{-2}$.[1] Neglecting possible falloff and isotope effects, Dzarnoski et al. estimated a value of the $(k_2/k_1)_{925K,\infty} = 0.23$ by single-pulse shock tube experiments of Si_2D_6.[2] These values have been considered as upper estimates. The recommended rate parameters for the reaction 2, which is used in the present simulations, were evaluated by combining the potential energy estimate of Gordon et al.,[49] the reaction rate data of Becerra and Walsh,[7] thermodynamics, and Arrhenius parameters for the other silane-like dissociation reactions and silylene insertion reactions.[10,16] Recently, Smirnov reexamined the two-channel decomposition of disilane using a model based on the solution of the one-dimensional master equation.[50] The falloff curves for $k_1(T)$ and $k_2(T)$ at three temperatures, 1200, 925, and 550 K, have been calculated by using experimental values of $k_1^\infty(T)$ and $k_2^\infty(T)$. Their results showed that under most of the practically interesting thermal conditions, the contribution of

the reaction channel 2 to disilane decomposition is small, about a few percent. However, no reliable values for $k_2^{\infty}(T)$ and $k_2(T)$ in the falloff region have been determined experimentally using direct methods. According to results of quantum chemical calculations of the potential energy surfaces for Si_2H_6 decomposition, both channels have no energy barrier and heats of reactions are also very similar, <2 kcal mol^{-1} (Table 1). Therefore, rather close values of $k_1(T)$ and $k_2(T)$ may be expected. A larger value of $k_2(T)$ may cause better agreement with the experimental profile of Si_2H_4. The experimental data measured by the direct methods should be necessary for the evaluation of $k_2(T,P)$. Thus, the discrepancy between the experimental and modeling results of Si_2H_4 concentration profiles would be related to incomplete rate parameters concerning Si_2H_4 formation and reduction processes or neglect of the heterogeneous reactions in the simulation or both.

Simulation results show that cyclic hydrogenated silicons (Si_nH_{2n}, Si_nH_{2n-2}, Si_nH_{2n-4}, etc.) become important in the formation of the higher hydrogenated silicon clusters. For example, the formation ratio of $[Si_nH_{2n}]/[Si_nH_{2n+2}]$ is larger than unity for Si_n ($n \geq 5$). This behavior is in qualitative agreement with the experimental results. We did not attempt a quantitative description of experimental results for other Si_nH_m species because the absolute concentrations of Si_nH_m species are unknown. The quantitative measurements for Si_nH_m are necessary for further discussion of the reaction mechanism of hydrogenated silicon clusters.

Conclusion

Disilane consumption and hydrogenated silicon cluster formation during disilane pyrolysis in a flow reactor have been analyzed by using mass spectrometry coupled with VUV photoionization. The formation of $Si_{2n}H_{2n}$, Si_nH_{2n-2}, and Si_nH_{2n-4} containing up to 10 silicon atoms, which have linear or cyclic and polycyclic structures, has been observed as the gas-phase products during disilane pyrolysis at reactor pressures of 20−40 Torr and temperatures of 680−860 K. The maximum signal originating from silicon hydride clusters was observed at approximately 750−800 K. The temperature- and time-dependences on the reduction of Si_2H_6 and the production of Si_nH_m were compared with the results of simulations based on a gas-phase kinetic mechanism proposed by Swihart and Girshick.[15] Si_2H_6 concentration profiles were reproduced reasonably by the kinetic model. The model was consistent with the experimental concentration trends for the silicon hydride clusters, except for Si_2H_4. The multi-H_2-elimination processes play an important role in the formation of higher hydrogenated silicon clusters. We have pointed out some of the areas in which more work is required, such as the experimental evaluation of the rate parameters of reaction 2, the quantitative analysis of Si_nH_m, and a model including radical-surface chemistry.

Acknowledgment. This work was supported in part by a Grant-in-Aid from the Ministry of Education, Science, Sports and Culture under Grant No. 11450297. We are grateful to Mark T. Swihart of State University of New York (SUNY) at Buffalo for providing us with the chemical kinetic model.

References and Notes

(1) Bowrey, M.; Purnell, J. H. *Proc. R. Soc. London, Ser. A* **1971**, *321*, 341.

(2) Dzarnoski, J.; Rickborn, S. F.; O'Neal, H. E.; Ring, M. A. *Organometallics* **1982**, *1*, 1217.

(3) Olbrich, G.; Potzinger, P.; Reimann, B. Walsh, R. *Organometallics* **1984**, *3*, 1267.

(4) Gordon, M. S.; Truong, T. N.; Bonderson, E. K. *J. Am. Chem. Soc.* **1986**, *108*, 1421.

(5) Martin, J. G.; Ring, M. A.; O'Neal, H. E. *Int. J. Chem. Kinet.* **1987**, *19*, 715.

(6) Martin, J. G.; O'Neal, H. E.; Ring, M. A. *Int. J. Chem. Kinet.* **1990**, *22*, 613.

(7) Becerra, R.; Walsh, R. *J. Phys. Chem.* **1987**, *91*, 5765.

(8) Becerra, R.; Walsh, R. *J. Phys. Chem.* **1992**, *96*, 10856.

(9) Moffat, H. K.; Jensen, K. F.; Carr, R. W. *J. Phys. Chem.* **1992**, *96*, 7683.

(10) Moffat, H. K.; Jensen, K. F.; Carr, R. W. *J. Phys. Chem.* **1992**, *96*, 7695.

(11) Ring, M. A.; O'Neal, H. E. *J. Phys. Chem.* **1992**, *96*, 10848.

(12) Yuuki, A.; Matsui, Y.; Tachibana, K. *Jpn. J. Appl. Phys.* **1987**, *26*, 747.

(13) Giunta, C. J.; McCurdy, R. J.; Chapple-Sokol, J. D.; Gordon, R. G. *J. Appl. Phys.* **1990**, *67*, 1062.

(14) Frenklach, M.; Ting, L.; Wang, H.; Rabinowitz, M. J. *Isr. J. Chem.* **1996**, *36*, 293.

(15) Swihart, M. T.; Girshick, S. L. *J. Phys. Chem. B* **1999**, *103*, 64.

(16) Ho, P.; Coltrin, M. E.; Breiland, W. G. *J. Phys. Chem.* **1994**, *98*, 10138.

(17) Weerts, W. L. M.; de Croon, M. H. J. M.; Marin, G. B. *J. Electrochem. Soc.* **1998**, *145*, 1318.

(18) (a) Onischuk, A. A.; Strunin, V. P.; Ushakova, M. A.; Panfilov, V. N. *Int. J. Chem. Kinet.* **1998**, *30*, 99. (b) Onischuk, A. A.; Levykin, A. I.; Strunin, V. P.; Ushakova, M. A.; Samoilova, R. I.; Sabelfeld, K. K.; Panfilov, V. N. *J. Aerosol Sci.* **2000**, *31*, 879.

(19) Simon, J.; Feurer, R.; Reynes, A.; Morancho, R. J. *J. Anal. Appl. Pyrolysis* **1992**, *24*, 51.

(20) (a) Johannes, J. E.; Ekerdt, J. G. *J. Appl. Phys.* **1994**, *76*, 3144. (b) Johannes, J. E.; Ekerdt, J. G. *J. Electrochem. Soc.* **1994**, *141*, 2135.

(21) Tonokura, K.; Murasaki, T.; Koshi, M. *Chem. Phys. Lett.* **2000**, *319*, 507.

(22) Wiley, W. C.; McLaren, I. H.; *Rev. Sci. Instrum.* **1955**, *26*, 1150.

(23) Mamyrin, B. A.; Karataev, V. I.; Shmikk, D. V.; Zagulin, V. A. *Sov. Phys.—JETP* **1973**, *37*, 45.

(24) Hilbig, R.; Wallenstein, R. *IEEE J. Quantum Electron.* **1981**, *QE-17*, 1566.

(25) Ruscic, B.; Berkowitz, J. *J. Chem. Phys.* **1991**, *95*, 2407.

(26) Kameta, K.; Ukai, M.; Terazawa, N.; Nagano, K.; Chikahiro, Y.; Kouchi, N.; Hatano, Y.; Tanaka, K. *J. Chem. Phys.* **1991**, *95*, 6188.

(27) Fuke, K.; Tsukamoto, K.; Misaizu, F.; Sanekata, M. *J. Chem. Phys.* **1993**, *99*, 7807.

(28) Berkowitz, J.; Green, J. P.; Cho, H.; Ruscic, B. J. *J. Chem. Phys.* **1987**, *86*, 1235.

(29) Ruscic, B.; Berkowitz, J. *J. Chem. Phys.* **1991**, *95*, 2416.

(30) Curtiss, L. A.; Raghavachaii, K.; Deutsch, P. W.; Pople, J. A. *J. Chem. Phys.* **1991**, *95*, 2433.

(31) Bock, H.; Ensslin, W.; Feher, F.; Freund, R. *J. Am. Chem. Soc.* **1976**, *98*, 668.

(32) Potzinger, P.; Lampe, F. W. *J. Phys. Chem.* **1969**, *73*, 3912.

(33) Frisch, M. J.; Trucks, G. W.; Schlegel, H. B.; Scuseria, G. E.; Robb, M. A.; Cheeseman, J. R.; Zakrzewski, V. G.; Montgomery, J. A., Jr.; Stratmann, R. E.; Burant, J. C.; Dapprich, S.; Millam, J. M.; Daniels, A. D.; Kudin, K. N.; Strain, M. C.; Farkas, O.; Tomasi, J.; Barone, V.; Cossi, M.; Cammi, R.; Mennucci, B.; Pomelli, C.; Adamo, C.; Clifford, S.; Ochterski, J.; Petersson, G. A.; Ayala, P. Y.; Cui, Q.; Morokuma, K.; Malick, D. K.; Rabuck, A. D.; Raghavachari, K.; Foresman, J. B.; Cioslowski, J.; Ortiz, J. V.; Stefanov, B. B.; Liu, G.; Liashenko, A.; Piskorz, P.; Komaromi, I.; Gomperts, R.; Martin, R. L.; Fox, D. J.; Keith, T.; Al-Laham, M. A.; Peng, C. Y.; Nanayakkara, A.; Gonzalez, C.; Challacombe, M.; Gill, P. M. W.; Johnson, B. G.; Chen, W.; Wong, M. W.; Andres, J. L.; Head-Gordon, M.; Replogle, E. S.; Pople, J. A. *Gaussian 98*, revision A.7; Gaussian, Inc.: Pittsburgh, PA, 1998.

(34) Becke, A. D. *Phys. Rev. A* **1988**, *38*, 3098.

(35) Lee, C.; Yang, W.; Parr, R. G. *Phys. Rev. B* **1988**, *41*, 785.

(36) Becke, A. D. *J. Chem. Phys.* **1993**, *98*, 5648.

(37) Baboul, A. G.; Curtiss, L. A.; Redfern, P. C.; Rassolov, V. J. *J. Chem. Phys.* **1999**, *110*, 7650.

(38) Kee, R. J.; Rupley, F. M.; Meeks, E.; Miller, J. A. *Chemkin-III: A Fortran Chemical Kinetic Package for the Analysis of Gas-Phase Chemical and Plasma Kinetics*; Sandia National Report No. SAND96-8216; Sandia National Laboratories: Albuquerque, NM, 1996.

(39) Becerra, R.; Frey, H. M.; Mason, B. P.; Walsh, R. Gordon, M. S. *J. Chem. Soc., Faraday Trans.* **1995**, *91*, 2723.

(40) Tada, N.; Tonokura, K.; Matsumoto, K.; Koshi, M.; Miyoshi, A.; Matsui, H. J. *J. Phys. Chem. A* **1999**, *103*, 322.

(41) Silylene ($HSi-Si_{n-1}H_{2n-1}$) and silene ($H_2Si=SiHSi_{n-2}H_{2n-3}$) are isomers in the Si_nH_{2n} species.

(42) *SENKIN: A Fortran Program for Predicting Homogenious Gas-Phase Chemical Kinetics with Sensitivity Analysis*; Sandia National

Laboratories Report No. SAND87-8248 Revised; Sandia National Laboratories: Albuquerque, NM, 1997.

(43) Verner, D. A.; Ferland, G. J.; Korista, K. T.; Yakovlev, D. G. *Astrophys. J.* **1996**, *465*, 487.

(44) Becerra, R.; Frey, H. M.; Mason, B. P.; Walsh, R. J. *J. Organomet. Chem.* **1996**, *521*, 343.

(45) Ali, M. A.; Kim, Y.-K.; Hwang, W.; Weinberger, N. M.; Rudd, M. E. *J. Chem. Phys.* **1997**, *106*, 9602.

(46) Krishnakumar, E.; Srivastava, S. K. *Contrib. Plasma Phys.* **1995**, *35*, 395.

(47) The heats of reaction were calculated using the G3//B3LYP level of theory.

(48) Gordon, M. S.; Bartol, D. *J. Am. Chem. Soc.* **1987**, *109*, 5948.

(49) Gordon, M. S.; Truong, T. N.; Bonderson, E. K. *J. Am. Chem. Soc.* **1986**, *108*, 1421.

(50) Smirnov, V. N. *Kinet. Catal.* **1997**, *38*, 309.